JVSTB
JOURNAL OF VACUUM SCIENCE AND TECHNOLOGY B

High-resolution complex structures for two-dimensional photonic crystals realized by x-ray diffraction lithography

L. Businaro, F. Romanato, P. Candeloro, E. Di Fabrizio, M. Patrini et al.

Citation: J. Vac. Sci. Technol. B **21**, 748 (2003); doi: 10.1116/1.1547726
View online: http://dx.doi.org/10.1116/1.1547726
View Table of Contents: http://avspublications.org/resource/1/JVTBD9/v21/i2
Published by the AVS: Science & Technology of Materials, Interfaces, and Processing

Related Articles

Nanofabrication of photonic crystal-based devices using electron beam spot lithography
J. Vac. Sci. Technol. B 29, 06FF06 (2011)

Coexistence of guided mode resonance and extraordinary optical transmission in metal/dielectric/metal photonic crystal slab
J. Vac. Sci. Technol. B 29, 06FF05 (2011)

Fabrication of two-dimensional tungsten photonic crystals for high-temperature applications
J. Vac. Sci. Technol. B 29, 061402 (2011)

Large area 3D helical photonic crystals
J. Vac. Sci. Technol. B 29, 06FF02 (2011)

Statistical analysis of subnanometer residual disorder in photonic crystal waveguides: Correlation between slow light properties and structural properties
J. Vac. Sci. Technol. B 29, 051601 (2011)

Additional information on J. Vac. Sci. Technol. B

Journal Homepage: http://avspublications.org/jvstb
Journal Information: http://avspublications.org/jvstb/about/about_the_journal
Top downloads: http://avspublications.org/jvstb/top_20_most_downloaded
Information for Authors: http://avspublications.org/jvstb/authors/information_for_contributors

ADVERTISEMENT

High-resolution complex structures for two-dimensional photonic crystals realized by x-ray diffraction lithography

L. Businaro,[a] F. Romanato, P. Candeloro, and E. Di Fabrizio
LILIT Lab.-INFM S.S.14, km 163.5, I-34017 Basovizza, Trieste, Italy

M. Patrini, M. Galli, and C. Andreani
Dipartimento di Fisica A. Volta, Università di Pavia Via Bassi, 6 I-27100 Pavia, Italy

A. Passaseo and M. De Vittorio
National Nanotechnology Lab INFM, Università di Lecce, Via Arnesano, I-73100 Lecce, Italy

(Received 28 May 2002; accepted 23 December 2002; published 6 March 2003)

Two-dimensional photonic band gap structures were fabricated by x-ray lithography combined with ion etching on metalorganic chemical vapor deposition grown GaAs/AlGaAs waveguides. Such structures, more amenable to fabrication than fully three-dimensional photonic crystals, allow the confinement of light in the third direction using index guiding. The feasibility of complex high-resolution (down to 50 nm) unit cell fabrication has been demonstrated by exploiting x-ray diffraction and nonlinear resist response during the development process. Optical characterizations of some samples were performed. These characterizations show the presence of well-defined photonic band gap structures and second harmonic property generation. The results have been discussed and compared with theoretical simulation. © *2003 American Vacuum Society.*
[DOI: 10.1116/1.1547726]

I. INTRODUCTION

A vast range of technological applications, including telecommunications, laser, television, radar, etc., is based on control of radiation fields. One of the most promising techniques to provide complete control on radiation are photonic crystals (PCs). Even though straightforward application of the photonic band gap (PBG) concept is generally thought to require three-dimensional (3D) photonic crystals,[1–4] much interest has been devoted to two-dimensional (2D) PCs. This is because 2D PCs are potentially more amenable to fabrication and much closer to application.[5] In the 2D case the confinement in the third direction can be achieved with the help of a planar waveguide.[6] However, definite standardization is still far from being achieved and different fabrication methods,[7–9] architectures, and integration strategies[10–12] of 2D PC are under investigation and in competition to produce first market devices.

Recent works[13,14] stress the importance of properly designing the lattice-unit cell shape in order to optimize the PBG and to control the polarization propagation more effectively. A second field where complex unit cells help, is for the application of PCs to second-harmonic generation (SHG).[15] In that case the need to obtain patterned materials with high filling factors (ratio between the dielectric volume and the air volume)[16,17] leads to the design of unit cells different both from holes and pillar that are commonly found when dealing with PCs. From the fabrication point of view, the control of unit cell shape with lateral resolution down to few tens of nanometers, with defect-free patterns and controlled periodicity on large areas, presents a challenging technological problem and no experimental investigation has been performed.

GaAs PCs slabs are very well suited for both light propagation control and SHG.[18,19] While the high refractive index of GaAs ($n=3.65$) allowed its wide use in photonic applications, SHG is a more complicated task due to the optical isotropy of this material. In fact, there are two key characteristics of materials to be used for SHG: the second order susceptibility, that is very high for GaAs, and the ability to match the phase velocities between the different frequencies.[20] (For GaAs $\chi^{(2)}$ 240 pm V^{-1}. This value gives about 1 order of magnitude greater efficiency than the commonly used materials.) Phase matching can be obtained, in birefringent materials, with a careful choice of the polarization for the different waves in order to adjust their phase velocities. In the isotropic GaAs phase matching is obtained by using an artificially built-in birefringence breaking the isotropy with the insertion of a AlGaAs film.[21] Moreover, SHG efficiency can be greatly enhanced (6 order of magnitude higher than bulk GaAs) by localized photonic eigenstates in 2D PCs.[22] As GaAs is the material of choice for semiconductor lasers, it could be possible to integrate optical sources and frequency converters in order to obtain new devices. Starting from relatively simple x-ray masks, a careful diffraction design of the projected pattern in x-ray lithography (XRL), together with the accurate choice of the exposure dose and of the development time (Sec. II), allowed us to achieve various complex patterns on the resists (Sec. III). The pattern transfer into GaAs waveguide was obtained through a dry etching process (Sec. IV). Optical characterization showed the presence of photonic bands and high efficiency in diffracted and reflected SHG signals (Sec. V).

[a]Electronic mail: luca.businaro@elettra.trieste.it

II. DESIGN

Entire families of symmetric complex patterns can be obtained by means of x-ray diffracted radiation. After choosing the desired unit cell and array structure, it is possible, using proper simulation tools and knowing the meaningful parameters of the x-ray beam, to design a relatively simple mask. The particular design characteristics of LILIT lab XRL beam line[23] allows the shaping of the spectrum to be delivered by our optical system by selecting the wavelength band pass. In the case of samples described in this work, we chose to work at the minimum wavelength spread that results in a spectrum centered at 0.83 nm (1.5k eV) with full width half depth of 0.56 nm (700 eV). To generate strong diffraction effects, the spatial coherence of the light must be larger than the typical dimension of the diffracting elements. According to the Van Cittert–Zernike theorem,[24] the spatial coherence length of the present beamline is

$$l_c^{\text{spatial}} = \frac{\lambda}{2\pi}\frac{L}{S} \cong 20 \ \mu\text{m},$$

obtained considering the beam line length $L=25$ m and by a vertical bending magnet source size $S=200$ μm. This is much larger than typical x-ray mask structures.

The aim of our experiment is to control the resulting diffraction pattern distribution and to generate complex lithographic structures. Simulations have been performed using the TOOLSET[25,26] code, which was developed specifically to model the exposure and the development of a resist in x-ray proximity lithography. The code first calculates the light transmission through the different layers and the near-field propagation of the electromagnetic field onto the resist, afterwards, it simulates development of the exposed resist. The program requires the knowledge of the parameters describing the x-ray source and x-ray mask. Therefore, input parameters are the natural divergence of the incoming beam, the angular, and the constant blur,[22] the layering of the mask and its pattern, the kind of resist (thickness, chemical composition, dissolution rate), the atmosphere where the exposure takes place, the exposure and development time, and finally the mask–substrate gap distance. After we imposed the physical parameters of the exposing beam and of the resist behavior, we investigated the mask–substrate gap distance parameter. In particular, we focused our attention on the condition for the fabrication of rings with or without central pillars generated by a mask consisting of an array of squares (Fig. 1). We chose this focus because of the relative simplicity of the mask and because of the interest of this kind of lattice both for PCs and SHG. In Fig. 2 we have reported the simulated aerial diffraction pattern obtained for a gap of 15 μm (i.e., one of the mask–wafer gaps used during the experiments). The simulation shows several peaks and valleys whose position and intensity are strongly dependent on the geometrical configuration of the lattice. We also report the diffraction pattern intensity along a cutting line of the mask. We note that the single strong minimum at the center of the transmitted beam is responsible for the dot at each lattice-unit base in Fig. 3(b).

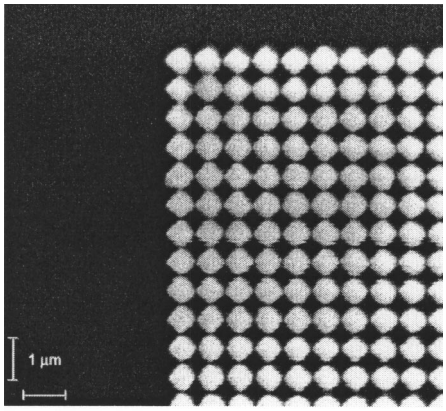

FIG. 1. SEM image of the XRL mask.

The diffraction is not the only effect that must be controlled to achieve the final lithographic pattern. In order to develop correctly the exposed resist an accurate optimization of the exposure dose and of the development time is required. This study has also been performed for exploiting the part of TOOLSET devoted to the resists development. We introduced the poly(methylmethacrylate) (PMMA) and SAL 601 resist dissolution rate[27] in order to compute the resist development time evolution on a representative area. As examples in Figs. 3(a), 3(b), and 3(c) we have reported the simulated SAL601 resist structures considering a mask substrate gap of 5, 10, and 15 μm, respectively, while in Fig. 3(d) we reported a simulated PMMA structure obtained simulating a gap of 15 μm. We note that, because of the

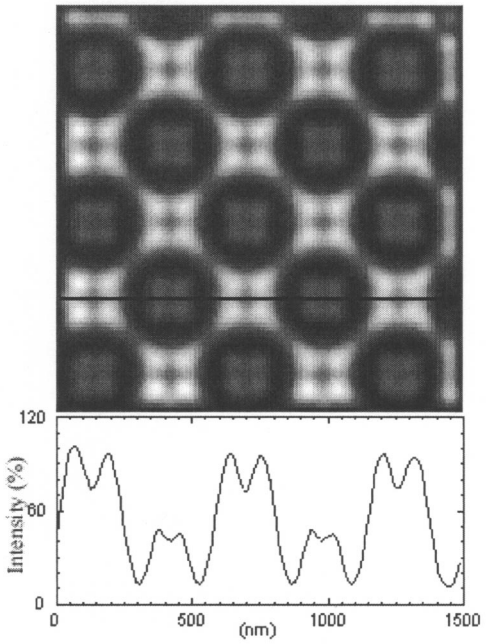

FIG. 2. Aerial diffraction pattern simulation generated by the x-ray mask pattern obtained with a 15 μm mask–substrate gap. The intensity profiles along the cut line on the aerial image appears on the bottom panel.

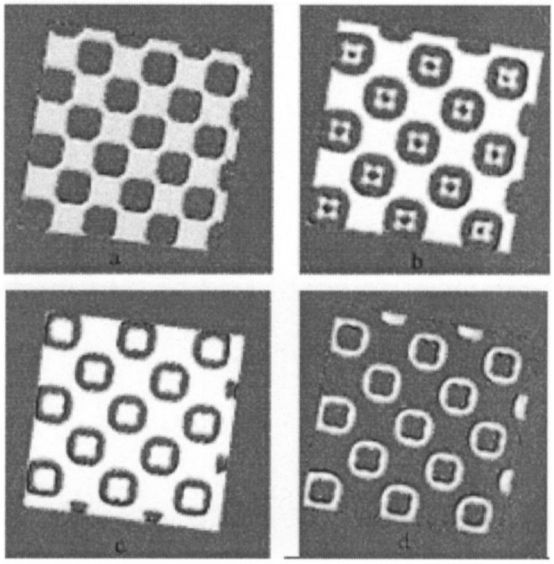

FIG. 3. Simulation of the developed SAL 601 and PMMA resists exposed at three different mask–substrate gaps: (a) SAL 5 μm, (b) SAL 10 μm, (c) SAL 15 μm, and (d) PMMA 15 μm.

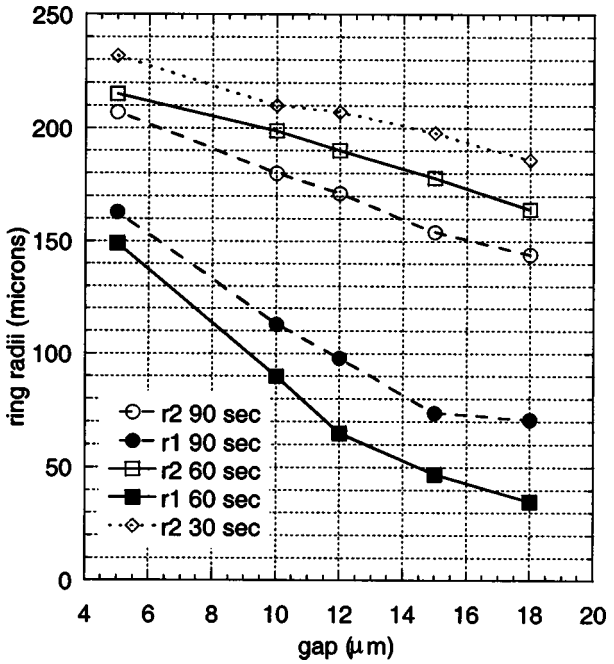

FIG. 4. Internal and external radius of the 2D lattice basis obtained for different mask–substrate gaps and developing times.

etching process used as the final step of fabrication, the simulation appears to be the negative of the final patterning on the samples.

By choosing the right experimental conditions, several combinations of internal and external radii of the rings or a controlled smoothing of the squared angles can be achieved. The key parameter in this case is the contrast between the absolute and local maxima (and minima) of the diffraction pattern (Fig. 2, lower part) that is high enough (more than 20%) to guarantee the modulation of the lithographic structures. The mask–substrate gap dependence of the internal and external diameter of rings for three different development times (30, 60, and 120 s) are reported in Fig. 4 for the PMMA resist and a dose of 3.5 J/cm^2. Results show that a large range of configurations can be achieved. At 30 s, no holes can be open in the base of the lattice. In contrast holes can be open in the base of the lattice at 60 s. A further increase of the development time decreases the external radius and increases the internal. This results in a thinning of the ring walls, if we consider the resist structure, the opposite happens for the etched structure. The structures of 50 nm ring wall thickness were considered the fabrication limit of this process.

III. FABRICATION

The samples studied in this work were grown in a horizontal low pressure metalorganic chemical vapor deposition system (AIXTRON 200 AIX) equipped with a rotating substrate holder using a growth pressure of 20 mbar. Trimethyl gallium (TMGa), trimethyl aluminum (TMAl), and pure arsine (AsH_3) were used as source materials. Palladium purified H_2 with a flow rate of 7 slm was the carrier gas. The growth was performed on (100) exactly oriented semi-insulating GaAs substrates at the nominal growth temperature of 750 °C. The structure consisted of 500 nm of GaAs as the topmost layer, followed by 1500 nm middle layer of $Al_{0.25}Ga_{0.75}As$, and 200 nm GaAs buffer layer. The whole structure was grown at the rate of 4 μm/h and unintentionally doped.

XRL masks were generated by electron-beam lithography over a 4×4 mm^2 area (Fig. 1). The pattern consists of a chessboard lattice of squares with a period of 500 nm along the diagonals. The pattern was exposed in a 400 nm thick film of PMMA spun on a Au/Cr-coated Si_3N_4 2-μm-thick membrane and prebaked at 170 °C on a hotplate. After development for 30 s in a 1:3 solution of methyl isobutyl ketone and isopropyl alcohol (MIBK:IPA), rinsing in IPA and 30 s O_2 plasma cleaning,[28] the patterned area was filled by electro-plating deposition with 350 nm of Au. The remaining PMMA was stripped in hot acetone at 50 °C.

The proximity x-ray lithography was performed at LILIT[29] beam line located at Elettra Synchrotron, Trieste. Four samples were coated with resists of both tones: PMMA with molecular weight 950 kDa with 7% of solid part (positive), and SAL 601 50% diluted in EC solvent (negative). 150 nm of PMMA was spun on the samples and prebaked at 170 °C on hot plate for 5 min. SAL 601 was spun at 200 nm and prebaked at 105 °C for 1 min. The most relevant exposure parameter was the mask–substrate gap that we selected on three values: 5, 10, and 15 μm.

The exposure doses were 2400 and 125 mJ/cm^2, respectively, for PMMA and SAL 601 samples. The latter were postbaked for 1 min at 105 °C on a hot plate. PMMA samples were developed for 45–50 s in a 1:3 solution of MIBK:IPA and rinsed in IPA. SAL 601 samples were developed for 5 min in MF312 diluted in H_2O and rinsed with demineralized water. The process was completed including a

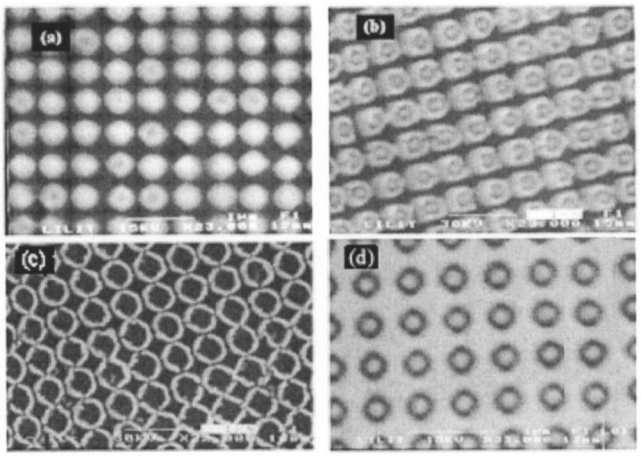

FIG. 5. Replicas of the x-ray mask and diffraction effects obtained by setting different gap distances: (a) sample S5: one-to-one replica; (b) sample S10: diffraction effects using SAL resist and a gap of 10 μm; 50 nm wide pillars have been generated on the center of the rings; (c) sample S15: array of dielectric rings SAL resist and gap of 15 μm; and (d) sample P15: array of air rings obtained using PMMA resist and a gap of 15 μm.

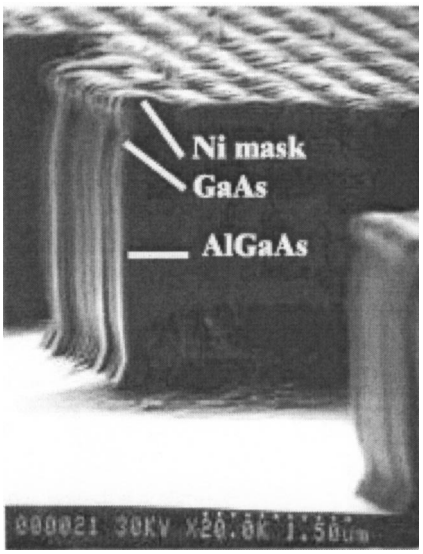

FIG. 6. Cross section of sample S15 where can notice the result of the reactive-ion etching process onto the sample surface.

reactive-ion etching (RIE) in oxygen at 5×10^{-2} Torr and a plasma power of 50 W to guarantee a complete cleaning of the bottom of the structures.

Finally, a liftoff process was performed by evaporating 50 nm of nickel followed by stripping the residual resist. Nickel showed an extremely high selectivity to the RIE performed by an inductively coupled plasma RIE reactor in a atmosphere of 95% $SiCl_4$ and 5% of Ar and a cathode bias voltage of 230 V. The etching rate was 0.39 μm/min. The typical total etching time of 5 min caused an etch depth of about 2 μm in the patterned regions as shown in Fig. 6.

IV. EXPERIMENT

Three samples prepared with SAL 601 and named S5, S10 and S15 were exposed with the mask–substrate gaps set, respectively, at 5 μm [Fig. 5(a)], 10 μm [Fig. 5(b)] and to 15 μm [Fig. 5(c)]. A fourth sample, P15,[30] which was spun with PMMA, was exposed at a 15 μm mask–substrate gap [Fig. 5(d)]. Note that Fig. 5 shows the result of the nickel mask obtained after the evaporation and stripping processes. The details of the cross-section 3D view of sample P15 (Fig. 6), selected as representative of all the other samples, show that the lithographic pattern has been effectively etched through the thickness of the epitaxial AlGaAs film. This provides structures with aspect ratios on the order of 7. Notice the layering of the epitaxial growth and the residual nickel film used as the mask layer during the RIE.

It is also worth noticing that the dependence of the lattice-unit cell on the mask–substrate gap distance follows the predictions of simulations presented in the last section. In the case of the 5 μm mask–substrate gap [Fig. 5(a)], the mask features are well reproduced. This is the case named ''proximity x-ray lithography'' where a one-to-one replica of the mask can be achieved and where the diffraction effects have been almost completely suppressed by minimizing the mask–substrate gap.

The diffraction effects, on the contrary, are evident on the samples exposed at the 15 μm mask–substrate gap with both negative and positive resist [Figs. 5(c) and 5(d)]. The square shape of the mask lattice-unit cell becomes strongly smoothed at the corners and the cell appears as a hole (or a pillar, depending on the tone of the resist) at the center. The patterning obtained exposing the negative resist appears to be composed of an array of rings with a remarkably thin lateral wall ($<$50 nm). In this case, the filling factor of the resulting photonic crystal, i.e., dielectric fraction on the total unit cell area, is very low and ranges from 9% for S15 to 28% for S5. Of course an opposite patterning with a very high filling factor, 78%, can be achieved using positive (PMMA) resist [Fig. 5(d)].This resist provides a final structure composed of thin rings etched into the epitaxial multilayer.

An even more complex case is shown by sample S10 exposed at the 10 μm mask–substrate gap [Fig. 5(b)]. In this case a further central pillar appears with a 100 nm wide diameter and 70 nm apart from the external ring, whose wall is 45 nm thick. It is remarkable that these high-resolution structures have been reproduced almost perfectly on a surface of 4×4 mm^2.

V. OPTICAL CHARACTERIZATION

The photonic-band structure was investigated by means of the surface coupling technique proposed by Astratov *et al.*[31] for III–V photonic crystals. This method relies on the observation of sharp resonances in the reflectance spectra of collimated light incident on the surface of the photonic crystal. Variable-angle specular reflectance was measured in the range 0.25–2 eV by a Fourier-transform spectrometer Bruker IFS66 at a spectral resolution of 1 meV. The angle of inci-

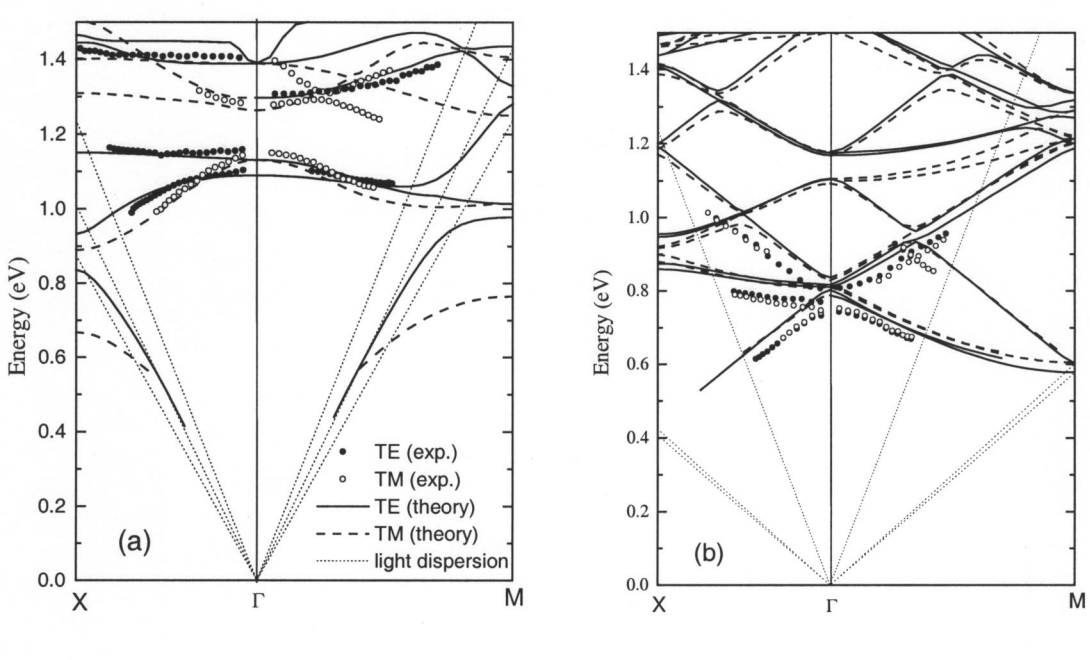

FIG. 7. Photonic band structure of sample S5 (a) and of sample P15 (b) as determined from experimental reflectance spectra (symbols) and from a theoretical calculation of photonic mode dispersion (lines). Light dispersion lines in air, GaAs, and AlGaAs are also reported (dotted lines).

dence θ was varied in the range 5°–60° with steps of 5° and angular resolution of ±1°. Measurements were taken for light incident along the Γ-*X* and Γ-*M* orientations of the samples, both in transverse electric and transverse magnetic polarizations and described in depth in Ref. 32.

Comparison between the obtained dispersion of the photonic bands and the results of a theoretical calculation shows that the latter reproduces all qualitative features of the photonic band dispersion with discrepancies from experimental data remaining below 0.05 eV.[33] As an example, the obtained dispersion of the photonic bands that spans the first Brillouin zone is shown in Fig. 7 for the S5 and P15 samples.

The present findings indicate that PCs with the same symmetry and the same film structure, but with very different dielectric fractions, show very different light-guide performance as shown in Figs. 7(a) and 7(b). The propagation losses of photonic modes have an intrinsic component, related to out-of-plane diffraction of quasiguided modes above the light line, and an extrinsic component arising from finite hole depth, roughness, inhomogeneities, etc. All these mechanisms contribute to diffuse scattering losses. The intrinsic mechanism of diffraction arises from the nonseparability of the dielectric tensor as a function of spatial coordinates, which produces a coupling of the quasiguided modes to the external radiation field. As follows from experimental and theoretical results, intrinsic diffraction losses are due to the increase with the air fraction.

For a given incidence angle and sample orientation, a second-harmonic beam is generated in all directions which satisfy the following conditions:

$$k\|' = 2k\| + G, \tag{1}$$

where $k\|(k\|')$ is the parallel wave vector of the incident (second-harmonic) beam and G is a reciprocal lattice vector of the photonic lattice. For $G=0$ we have the usual SHG in reflection. One can view the diffracted SH beam [$G\neq 0$ in Eq. (1)] as being due to SHG in reflection followed by diffraction at the harmonic frequency, or else diffraction at the pump frequency followed by SHG: the two processes are physically indistinguishable.

The SH signals detected both in reflection and in diffraction follow a quadratic law in the input fluence. The nonlinear radiation appears to be spatially coincident with the pump laser beam in reflection. The SH diffracted signals have been measured both for *s* and *p* polarization of the incident radiation and both for the Γ-$X(\phi=0°)$ and Γ-$M(\phi=45°)$ PC orientations and shown in Fig. 8. We also report the theoretical nonlinear SH diffraction curves derived from Eq. (1) for the two cases. Agreement between the experimental results and the theoretical curves is very good. Uncertainties over incidence angles are 1°, due to the alignment procedure both of the sample and of the incident laser beam. In our setup, the optical-fiber angular position is not absolutely calibrated but is obtained by measuring the position of the SH-reflected signal. Thus the uncertainty on the incident angle is directly transferred to the SH-reflected and diffracted beams.

For both reflected- and diffracted-SH measurements, the nonlinear reflection/diffraction coefficients, defined as $R^{NL}_{(R,D)}=I_{(R,D)}(2\omega)/I(\omega)^2$, have been evaluated. A value of the order of $\sim 5\times 10^{-24}$ m^2 M^{-1} for *s*-polarization and Γ-*X* crystal orientation is obtained and compares favorably with the theoretical prediction[34] of 5×10^{-24} m^2 W^{-1} for bulk

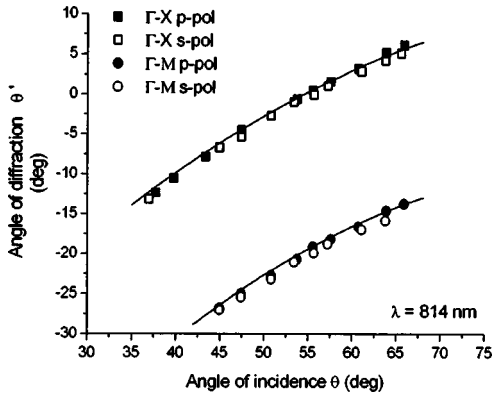

FIG. 8. Measured (dots) and calculated (lines) angles of diffraction for the angle $f=0°$ (Γ-X) and $f=45°$ (Γ-M) crystal orientation in the plane of incidence for the two polarizations as a function of the angle of incidence q of the pump beam onto the photonic crystal. The pump wavelength is 814 nm.

GaAs [1,0,0] crystal. Similar, consistent values have been obtained also for p polarization ($\sim 1\times 10^{-22}$ m^2 W^{-1} with Γ-M crystal orientation both for theoretical and experimental results). Indeed, the air filling factor of the photonic crystal amounts to only 12% in this sample, leading to a quasibulk GaAs [1,0,0] nonlinear response. In fact second harmonic reflected signal in p polarization is greater than that in s polarization, while in s polarization, Γ-M signals ([0,1,0] azimuth GaAs orientation) are lower than Γ-X ones ([1,1,0] azimuth GaAs orientation) and in p polarization the trend is opposite. Further experiments are under development in order to demonstrate SHG enhancement using phase matching in 2D PCs.

VI. CONCLUSIONS

Diffraction effects on x-ray lithography were exploited to generate 2D photonic crystals with complex unit-cell lattices. A high spatial degree of coherence and precise control of the mask–substrate gap distance are the crucial parameters that allow generating strong modulated illumination patterns on the resist. Computer simulations have shown that even when starting from a relative simple mask made of squares on a square lattice, rhombs or four-leaf clover patterns can be generated. In order to avoid any complication due to shape dependence, we focused on the fabrication of rings and antirings, with or without concentric pillars or holes, 2D photonic crystals on an air/GaAs/AlGaAs waveguide. The size modulation of the internal ring and of the eventual central pillar was achieved by exploiting the exposure dose and the resist development-time calibration. Wall rings as small as 50 nm and central pillars of 100 nm have been realized on 4×4 mm^2 areas.

The optical characterization has shown that fabricated 2D photonic crystals have definite optic-band structures and behave as SH generators. This technique can be applied to investigate the influence of the unit-cell lattice shape on the optical characteristics of the photonic crystals. In this work, we focused on the influence of the filling factor. The present findings indicate that samples with very low air fraction indeed have narrow reflectance structures arising from well-defined photonic modes. Therefore these modes must have small radiative linewidths and low propagation losses.

Presented at the 46th International Conference on Electron, Ion, and Photon Beam Technology and Nanofabrication, Anaheim, CA, 28–31 May 2002.

[1]M. Campbell, D. N. Sharp, M. T. Harrison, R. G. Denning, and A. J. Turberfield, Nature (London) **404**, 53 (2000).
[2]Y. A. Vlasov, X.-Z. Bo, J. C. Sturm, and D. J. Norris, Nature (London) **414**, 289 (2001).
[3]J. E. G. J. Wijnhoven and W. L. Vos, Science **281**, 802 (1998).
[4]S. Shoji and S. Kawata, Appl. Phys. Lett. **76**, 2668 (2000).
[5]D. L. Bullock, C. Shih, and R. S. Margulies, J. Opt. Soc. Am. B **10**, 399 (1993).
[6]S. G. Johnson, S. Fan, P. R. Villeneuve, J. D. Joannopoulos, and L. A. Kolodziejski, Phys. Rev. B **60**, 5751 (1999).
[7]T. F. Krauss and R. M. De La Rue, Prog. Quantum Electron. **23**, 51 (1999).
[8]C. C. Cheng, A. Scherer, and R. Chung, J. Vac. Sci. Technol. B **15**, 2764 (1997).
[9]E. Chow, S. Y. Lin, S. G. Johnson, P. R. Villeneuve, J. D. Joannopoulos, J. R. Wendt, G. A. Vawter, W. Zubrzycki, H. Hou, and A. Alleman, Nature (London) **407**, 983 (2000).
[10]O. Painter, R. K. Lee, A. Scherer, A. Yariv, J. D. O'Brien, P. D. Dapkus, and I. Kim, Science **284**, 1819 (1999).
[11]T. F. Krauss and R. M. De La Rue, Appl. Phys. Lett. **68**, 1613 (1996).
[12]J. Moosburger, M. Kamp, F. Klopf, M. Fuscher, and A. Forchel, Microelectron. Eng. **57–58**, 1017 (2001).
[13]R. Wang, X.-H. Wang, B.-Y. Gu, and G.-Z. Yang, J. Appl. Phys. **90**, 4307 (2001).
[14]S. Noda, M. Yokoyama, M. Imada, A. Chutinan, and M. Mochizuki, Science **293**, 1123 (2001).
[15]I. Freund, Phys. Rev. Lett. **21**, 1404 (1968).
[16]D. Labilloy *et al.*, Phys. Rev. Lett. **79**, 4147 (1997).
[17]H. Benisty *et al.*, J. Lightwave Technol. **17**, 2063 (1999).
[18]T. F. Krauss, R. M. De La Rue, and S. Brand, Nature (London) **383**, 699 (1996).
[19]Nonlinear Optics of Photonic Crystals, edited by C. M. Bowden and A. M. Zheltikov, feature issue, J. Opt. Soc. Am. B **19**, 1961–2296 (2002).
[20]J. A. Armstrong, N. Bloembergen, J. Ducuing, and P. S. Pershan, Phys. Rev. **127**, 1918 (1962).
[21]A. Fiore, V. Berger, E. Rosencher, P. Bravetti, and J. Nagle, Nature (London) **391**, 463 (1998).
[22]A. R. Cowan and J. F. Young, Phys. Rev. B **65**, 085106 (2002).
[23]E. Di Fabrizio, A. Nucara, M. Gentili, and R. Cingolani, Rev. Sci. Instrum. **70**, 1605 (1999).
[24]Hecht, *Optics* (Addison-Wesley, New York, 1998).
[25]M. Khan, L. Mohammad, J. Xiao, L. Ocola, and F. Cerrina, J. Vac. Sci. Technol. B **12**, 3930 (1994).
[26]M. Khan, B. S. Bollepalli, and F. Cerrina, University Wisconsin-Madison Report, 1997.
[27]M. Khan, S. B. Bollepalli, and F. Cerrina, Proceedings MSM Conference, Tokyo, Japan, 21–23 July 1997.
[28]SISTEC RIE 600 system.
[29]F. Romanato, E. Di Fabrizio, L. Vaccari, M. Altissimo, D. Cojoc, L. Businaro, and S. Cabrini, Microelectron. Eng. **57–58**, 101 (2001).
[30]The letter of the sample names indicates the resist and the number indicates the mask–substrate gap.
[31]V. N. Astratov, D. M. Whittaker, I. S. Culshaw, R. M. Stevenson, M. S. Skolnick, T. F. Krauss, and R. M. De La Rue, Phys. Rev. B **60**, R16225 (1999).
[32]M. Galli, M. Agio, L.C. Andreani, L. Atzeni, D. Bajoni, G. Guizzetti, L. Businaro, E. Di Fabrizio, F. Romanato, and A. Passaseo, Eur. Phys. J. B **27**, 79 (2002). Sample S5 and sample P15 have been already described in the present reference where they were named, respectively, RUN3 and L2.
[33]L. C. Andreani and M. Agio, IEEE J. Quantum Electron. **38**, 891 (2002).
[34]M. Falasconi, Thesis, University of Pavia, 2002.